ERJ
Engineering Research Journal
Faculty of Engineering
Minoufiya University

INVESTIGATIONS OF A TWO DIMENSIONAL JET IMPINGING ON TWO FLAT PLATES WITH AN ANGLE BETWEEN THEM

A. Abdel-Fattah , F.Sh Abou-Taleb , and Gamal H. Moustafa

Dept. of Power Mech. Eng., Faculty of Eng., Minoufiya University, Shebin El-Kom, EGYPT

ABSTRACT

Jet Impingement on two flat plates with an angle between them has been experimentally and Numerically studied at different flow and geometrical conditions. The numerical simulations were performed by the solution of Navier-Stokes equations with a k- ε model. The stagnation pressure ratio (p_o / p_a) was varied from 1.2 to 3. Thus, the Reynolds number based on the nozzle width (b) was ranged from 4.5 x 10^4 to 8.3 x 10^5 . The distance between the center of the two plates and nozzle exit plane (h/b) was changed from 5 to 60. The angle between the two plates (θ) was varied from 50° to 180° . Pressure distributions along the two plates were compared with those of a free jet. Also, results have been compared with those obtained from the numerical solution. It is concluded that the jet flow behavior and pressure distributions are more sensitive to the initial stagnation pressure, the impingement distance than those obtained with varying the angle between the two impingement plates. Comparison of the predicted behavior of the jet with those obtained from experimental results gives a good agreement.

يقدم البحث دراسة عملية ونظرية لسريان من الهواء (نفث) عند سرعات مختلفة يصطدم بجدارين بينهما زاوية، أستخدم هواء جاف مضغوط بقيم تتراوح بين ١,٢ – ٣ ضغط جوي محكوم بوسائل تحكم كي تعطي السرعات المطلوبة أثناء تمدد السريان خلال البوق ذات الشكل المستطيل ونتج من ذلك أن رقم الرينولدز تراوح بين ٤,٥ × ١٠^{٤} – ٨,٣ × ١٠^{٥} ، وتم تغيير الزاوية بين الجدارين من ٥٠ ° إلى ٩٠ ° وقورنت بالنتائج عندما كانت الزاوية بين الجدارين ١٨٠ ° ، واستخدم في الدراسة النظرية معادلات (Navier-Stokes with k-ε model) وتمت الدراسة مع تغير المسافة بين مخرج البوق والجدار وقورنت النتائج المسجلة بتلك في حالة عدم وجود جدار أي النفث الحر، وكان هناك اختلاف واضح ومؤثر بين شكل وتكوين مراحل تطور النفث عند اصطدامه بالجدارين مقارنة بالنفث الحر، واتضح من الدارسة أن شكل وتكوين النفث بعد الاصطدام بالجدارين بينهما زاوية يعتمد على المسافة بين مخرج البوق والجدار والسرعة الابتدائية للنفث وكذلك الزاوية بيت الجدارين، دراسة توزيع السرعات الناتجة من اصطدام النفث بالجدارين أعطى صورة واضحة المعالم عن تطور النفث وتأثير الزاوية بين الجدارين، ومقارنة النتائج العملية والنظرية أعطت توافق جيد،

Keywords: jet, impingement surface, Navier Stokes, K- ε model, Pitot tube

Nomenclature

c_1 , c_2 , c_3 , c_D , σ_k σ_ε empirical constants in the turbulence model
b : width (small dimension of nozzle)
h : Impingement distance
k : Turbulent Kinetic energy
L : length (long dimension of nozzle)
p : pressure
R : gas constant
S_ϕ : Source term
V_o : mean velocity at nozzle exit
u , v : velocity components along x, y
x,y : x and y directions
y : distance from the nozzle exit plane
Re : Reynolds number ($\rho V_o b / \mu$)
ρ : density
μ : Dynamic viscosity
ε : dissipation rate
Γ_ϕ : Diffusion coefficient
θ : angle between the two plates
T : temperature
ϕ : general dependent variable

Subscripts

a : Ambient condition
o : Stagnation condition
t : total condition
w : wall condition

1. INTRODUCTION

Impinging jet flows are widely used in many engineering applications such as the drying of film and textile, the cooling of hot steel plates, gas turbine cascade and combustor components. Recently, it is also used for cooling the microelectronic components. In fact, this is due to the enhancement of the high heat and mass transfer rates that occur in the impingement region. For Vertical Take – Off and Landing (VTOL) aircrafts, an important consideration is the aerodynamic interaction between air frame under surfaces and the ground.

The main structure of the impinging jet is defined by three main regions, Hwang and Liu (1989). The first jet part is the free jet region where the flow is the same as that of a jet issuing into an unbounded medium. The second part is the impingement region in which the large pressure enhances the change of flow direction. The third part is the wall jet region where the flow moves over the ground plane with constant pressure.

Most of previous studies have been performed the effect of jet impingement on flat surfaces, Colucci and Viskanta (1996), Phares, et. al. (2000). Impingement surfaces of more complex geometries such as cylindrical surfaces were investigated by Parneix, et. al. (1999) and Cornaro, et. al. (1999). Some of the earliest reports that do focus on jet impingement on curved surfaces are given by Chupp, et. al. (1969), who studied the heat transfer from an array of small round jets impinging on a concave surface. Tabakoff and Clevenger (1972) compared the cooling of a single slot jet with an array of round jets on a concave surface. Hrycak (1981) studied the heat transfer from concave hemispherical plates with the range of Reynolds number from 1.2×10^4 to 8.8×10^4 . Lee and Lee (1997) investigated the effect of surface curvature on the local heat transfer from a round jet.

It is well known that the flow structure of an impinging jet produced by an orifice or a nozzle is very complex, due to the generation of vortices, ambient entrainment, separation, and interaction with impingement and/or confining walls. After impingement the flow develops as a wall jet until it interacts with a confining wall. Hence, there are a number of parameters to be considered in the design of such systems: the distance between the nozzle and impingement surfaces, the flow rate, the initial flow conditions, the initial turbulence level and the overall geometry of the system. Gardon and Akfirat (1965) investigated the effect of turbulence on the heat transfer augmentation by controlling free stream turbulence at the nozzle exit. Tam and Norum (1992) studied the impingement tones of large aspect ratio supersonic rectangular jets. Lytle and Webb (1994) measured flow structures and local heat transfer rates at the value of nozzle to plate spacing less than one nozzle diameter and found peculiar behavior not evident at higher impingement distances. Lee et. al. (1994) investigated the local heat transfer characteristics of an elliptic impingement jet with an orifice nozzle having an aspect ratio of 2.14. Chen, et. al. (2000) studied the high Schmidt mass transfer in a laminar impinging slot jet flow for the Reynolds number from 220 to 690.

The objective of the present work is to study the behavior of the flow field of an air jet impinging on two flat plates with an angle between them. The stagnation pressure was varied to change the initial flow Reynolds number from 4.5×10^4 to 8.3×10^5 . Measurements of the wall and total pressures were made in the x and y directions. The distance between the nozzle exit and the impingement surfaces was varied from 5 to 60 nozzle width. The angle between the two plates was changed from 50° to 180°. Navier – Stokes equations with a k- ε model were used to perform the structure of flow field. Numerical work based on the SIMPLE procedure outlined by Patankar (1970) was utilized. A comparison between the theoretical and experimental results is given. The behavior of the impinging jet is also compared with the free jet.

2. EXPERIMENTAL SET UP AND PROCEDURE

The schematic diagram of the experimental set up is given in Fig.1. A high pressure blow down air supply system was used to produce the jet. Compressed dry air was discharged from two air compressors to an air tank of 8.3 m^3. The maximum pressure in the air tank was automatically controlled to within 8 bar. Then, the compressed air was passed through a 3`` diameter pipeline to restored in a settling chamber whose dimensions are 1.75 m long and 0.8 m in diameter. The pipeline control section includes a gate valve followed by a pressure regulating valve. Two mesh wire screens were fixed in the settling chamber to reduce the air disturbances and make the flow uniform at the nozzle exit. A rectangular convergent nozzle made of Aluminum with 35 mm length, 30 x 3 mm^2 at inlet, and 12 x 3 mm^2 at exit was attached to the settling chamber which was kept parallel to the ground floor. The air was accelerated through the nozzle and then released into the ambient atmosphere in the form of a free jet. The air jet was allowed to impinge on two flat surfaces made of Perspex. The dimensions of the two plates are 600 mm long and 300 mm width. The impingement surface was placed perpendicular to the flow direction. The angle between the two plates was changed from 50° to 180° , Fig. 1.

Measurements of wall and total pressures were made at different values of stagnation pressure from 1.2 to 3 atmospheres. The corresponding Reynolds number based on the nozzle exit width was ranged from $4.5\text{x}10^4$ to $8.3\text{x}10^5$. The wall pressure was measured through tabs of 0.5 mm inner diameter made along the impingement surfaces. The uncertainty in the tap location in all direction was ± 0.4%. The total pressure was measured by using a pitot tube with an inner diameter of 0.5 mm. The pitot tube was positioned on a three dimensional traversing mechanism with a pitch of 1 mm in all directions. The spatial resolution of the traverse system is 0.5 mm in all directions which is approximately 4 % of b. Water and Mercury U-tube manometers were connected to the pitot tube and pressure tabs that can help for pressure reading with an accuracy of ± 0.65 %. The stagnation pressure in the settling chamber was measured using a digital manometer, with uncertainty of ± 0.36 % . The distance between the surface and nozzle exit (the impingement distance, h/b) was varied from 5 to 60 with uncertainty of 2 %. The stagnation temperature in the settling chamber was measured using a digital thermometer whereas; a mercury thermometer was used to measure the ambient temperature (T). The temperature reading was uniform with an accuracy of ± 0.5 °C. The ambient atmospheric pressure was measured using a barometer with an accuracy of about ± 0.25 %. The nearest walls were kept sufficiently far from the tunnel to exclude their effects.

3. MATHEMATICAL MODELS

The transport equations representing the conservation of mass, momentum, turbulent kinetic energy and turbulent dissipation rate of the isothermal flow are cast into a general form of Cartesian Coordinates, Khodadadi and Vlachos (1989) :

$$\left[\frac{\partial}{\partial x}(\rho u\phi)+\frac{\partial}{\partial y}(\rho v\phi)\right]=\left\{\frac{\partial}{\partial x}\left(\Gamma_\phi\frac{\partial\phi}{\partial x}\right)+\frac{\partial}{\partial y}\left(\Gamma_\phi\frac{\partial\phi}{\partial y}\right)\right\}+S_\phi(x,y) \qquad (1)$$

where ϕ represents one of the following entities 1, u, v, k , and ε in which the dependent variables are: x-direction velocity u, y-direction velocity v, turbulent kinetic energy k and its dissipation rate ε . Γ_ϕ and S_ϕ stand for the corresponding effective diffusivity and source term, respectively. The corresponding expressions of Γ_ϕ and S_ϕ are given in Table 1, Khodadadi and Vlachos (1989).

Table 1 continuity, x-momentum, y-momentum, turbulent kinetic energy, and energy dissipation rate equations

ϕ	Γ_ϕ	S_ϕ
1	0	0
u	μ_{eff}	$-\frac{\partial P}{\partial x}+\frac{\partial}{\partial x}\left(\mu_{eff}\frac{\partial u}{\partial x}\right)+\frac{\partial}{\partial y}\left(\mu_{eff}\frac{\partial v}{\partial x}\right)-\frac{2}{3}\frac{\partial}{\partial x}\left(\mu_{eff}\left(\nabla\cdot\vec{V}\right)+\rho k\right)$
v	μ_{eff}	$-\frac{\partial P}{\partial y}+\frac{\partial}{\partial x}\left(\mu_{eff}\frac{\partial u}{\partial y}\right)+\frac{\partial}{\partial y}\left(\mu_{eff}\frac{\partial v}{\partial y}\right)-\frac{2}{3}\frac{\partial}{\partial y}\left(\mu_{eff}\left(\nabla\cdot\vec{V}\right)+\rho k\right)$
k	μ_{eff}/σ_k	$G_k-\rho\varepsilon$
ε	$\mu_{eff}/\sigma_\varepsilon$	$\frac{\varepsilon}{k}\left[c_1G-c_2\rho\varepsilon\right]+(1-c_3)\rho\varepsilon\left(\nabla\cdot\vec{V}\right)$

where

$$G_k=\mu_{eff}\left\{2\left[\left(\frac{\partial u}{\partial x}\right)^2+\left(\frac{\partial v}{\partial y}\right)^2\right]+\left(\frac{\partial u}{\partial y}+\frac{\partial v}{\partial x}\right)^2\right\}-\frac{2}{3}\left(\nabla\cdot\vec{V}\right)\left[\mu_{eff}\left(\nabla\cdot\vec{V}\right)+\rho k\right]$$

and

$$\mu_{eff}=c_D\frac{\rho k^2}{\varepsilon}+\mu$$

The turbulent constants are given as, Khodadadi and Vlachos (1989) :

$c_1 = 1.44$, $c_2 = 1.92$, $c_3 = 1.373$, $c_D = 0.09$, $\sigma_k = 1$, $\sigma_\varepsilon = 1.3$

3.1. Boundary Conditions and Solution Procedure

The flow at the nozzle exit was assumed to be fully developed; i.e., the axial gradients of all variables were set to zero. Thus, the boundary conditions were cast as follows, Fig.2 :

a) Inlet boundary (A – E)

$$v=V_o,\ k_o=0.04V_o^2,\ \varepsilon_o=\frac{c_D k_o^{1.5}}{0.1b}$$

b) At outlet (C – D)

$$\frac{\partial\phi}{\partial y}=0,\ and\ \phi=u,v,k..and..\varepsilon$$

c) Symmetry axis (A – B)

At the symmetrical plane, the normal gradient of all variables were set to zero and the velocity normal to this plane was also null, i.e., u = 0,

$$\frac{\partial\phi}{\partial y}=0..and..\phi=v,k..and..\varepsilon$$

d) At solid wall (B - C)

At solid walls, there is no slip and the law of the wall suggested by Chiu and Kuo (1995) was used to modify the flow parameters, i.e.,u, v, and ε .

The mathematical models consist of a set of differential equations subject to appropriate boundary conditions. To provide the algebraic form of the governing equations, a fully staggered grid system was adopted for the velocity components and scalar variables. These equations were discretized using a control volume finite difference methods (CVFDM). The numerical solution was accomplished by utilizing a version of semi-implicit method for Pressure Linked Equation model (SIMPLE) derived by Patanker (1970). In this algorithm, the velocity component u was calculated at the east and west faces of the main control volumes from the solution of u momentum equations, Fig.2. Similarly, the velocity component v were obtained at the north and south faces of the main control volume. Then, the pressure correction equation was solved, and velocity and pressure fields were corrected. To complete the iteration, the turbulent kinetic energy and energy dissipation rate equations were solved successively. The discretization equations were solved by the line–by line procedure, which is a combination of Gauss Seidel and the tridiagonal matrix algorithm in the stream-wise direction. The tridiagonal matrix algorithm (TDMA) was used to solve a set of discretization equations in the cross stream direction. Relaxation factors were employed to promote smooth convergence of the discretized equations. The relaxation factors were 0.5, 0.5, 0.3, 0.8, and 0.8 for u, v, p, k, and ε respectively. The turbulent viscosity was under-relaxed at a value of 0.8 . The converged criterion in this study was based on the successive changes in variables. All field variables were monitored, and the following condition was used to declare the convergence:

$$Max\left|\frac{\phi_{i,j}^{n}-\phi_{i,j}^{n-1}}{\phi_{i,j}^{n}}\right| \le 1x10^{-4} \qquad (2)$$

In addition, the ratio of the difference between the inlet mass flow rate and the outlet mass flow rate to the inlet mass flow rate was also examined. Convergence was declared if the relative mass imbalance was less than 1×10^{-3} and the Eq. (2) was satisfied simultaneously. To verify the algorithm, numerical tests were performed. Thus, 90 x 90 grids were placed non-uniformly in the computational domain. The x-direction (stream-wise) grid was fine under the jet, and the grid size was multiplied by a factor of 1.04 for the region between the jet and the downstream domain. The y-direction grid was chosen non-uniform, where the finest grids were set near the solid wall and expanded outward by power low formulation with a factor of 1.06.

4. RESULTS AND DISCUSSION

The features of the impinging jet was studied experimentally and numerically for different flow and geometrical conditions. Sample of data are presented as pressure distributions and contours of u, v, and k .

The total pressure distribution of a free jet for $p_o/p_a = 1.3$ is shown in Fig.3 for different locations downstream from the nozzle exit plane. At y/b = 5, the total pressure has a tophat profile, and the shear layer is very narrow. The jet core narrows with x, but exists up to an axial location $y/b \le 5$. After this location on downstream the total pressure has a bell shape. Note that there exists a small region of lower total pressure near the jet periphery, where the total pressure is slightly smaller than the ambient pressure. This behavior, most evident for $5 \le y/b \le 10$, is believed to be due to the low pressure core of the small vortices. As the distance from the nozzle exit increases the total pressure at the jet axis decays at higher rates, displaying more fluid entrainment and enhancing mixing. This is because the rectangular jet spreads in the minor axis plane more than in the major axis plane, resulting in a crossover point at which the jet becomes locally quasi-axisymmetric. Downstream of this point the major axis becomes the minor one, and vice versa, Colucci, D.W., and Viskanta (1996). In Fig.4, the wall pressure distributions for a jet impinging on a flat plate ($\theta = 180^{\circ}$) is given for comparison. The effect of the impingement surface is clearly observed between x/b = 1.75 and 6. At closed zone of the jet, $h/b \le 20$, the negative pressure is performed near the jet periphery. As the jet moves along the wall the static pressure equals the ambient pressure.

The effect of stagnation pressure on the wall pressure distribution along the two plates is given in Fig. 5, for h/b = 32 and $\theta^{\circ} = 50, 70, 90$. At the center of the plate, the wall pressure is maximum and has a tophat profile. It decreases as the flow moves along the surface in the x-direction. The spreading of the jet (jet width) increases as the jet propagates, indicating the higher mixing rate with the ambient fluid. At the end of the plate, the wall pressure equals the ambient pressure. Also, at the center of the plate, the maximum pressure increases as the stagnation pressure is increased. At the lower values of stagnation pressure, the negative pressure is also evident near the jet periphery. This behavior is not clearly seen with increasing the distance between the nozzle and impingement surface (h/b = 57), Fig.6. In this figure, the maximum pressure also decreases displaying the higher decay rate while the jet width increases, the spreading of the jet increases. The similarity between the two impingement distances is excellent, for all values of θ. This indicate that the pressure distributions is less sensitive to the change of the angle between the two plates compared to the change of stagnation pressure. A comparison with the

result of a flat plate ($\theta = 180^\circ$), Fig.4 indicates that the angle existed between the two plates damps the reflection effect of the impingement surface.

Fig. 7 shows the comparison between the theoretical and experimental results for different values of stagnation pressure. The data are given for $\theta = 50^\circ$ and 90°, h/b = 21.33 and 38. The agreement between them is good. The difference between the theoretical and experimental results near x/b = 2 for $\theta = 50^\circ$ is due to the reflection of the jet from the wall. This difference is not shown when the angle between the two plate is increased. Also, the difference has not evident for higher values of h/b, (h/b = 38). Both the experimental and theoretical results show that the peak values of wall pressure occur at the center and the pressure that to be lower than the ambient pressure occurs at the periphery of the jet. In Fig.8, the effect of the angle between the two plates θ on the pressure distributions is given for p_o = 1.3 and 2.5 atmospheres and h/b = 21.33 and 31.33. The pressure profile symmetry is excellent. The peak of the static pressure at the center of the plate increases with increasing the stagnation pressure. The agreement between the theoretical and experimental results is evident for all values of θ. Also, the negative pressure at the jet periphery covers more distance on the plate surface and the similarity of the pressure profiles has not affected by the change of the angle θ.

Fig. 9 indicates the effect of nozzle to plate spacing on the pressure distributions, for $\theta = 50^\circ$ and 90°. For all nozzle to plate spacings studied the pressure distributions are a maximum at the stagnation point. As x/b increases, the pressure decreases and approaches the ambient pressure for large x/b. The pressure is observed to become sub-atmospheric and reach a minimum at x/b = 2 and then increases to ambient pressure at x/b = 3. This pressure recovery is due to the momentum conservation at the impingement surface. The maximum pressure decreases (decay of the jet increases) with increasing the distance between the nozzle and plate while the spreading (jet width) increases. This is due to the ambient entrainment.

The contours of the velocities u, v and kinetic energy k are given in Fig. 10, for a jet impinging on a flat plate ($\theta = 180^\circ$ and h/b = 21.33). These results indicate that the numerical solution has reproduced the expected physical features of the jet interaction with the solid wall. The stagnation point, re-circulation zone, reflection, entrainment are clearly visible. The physical features of the jet are changed with using the two plates with an angle between them, Fig.11. The butterfly shape is dominated which is not evident within the case of the flat plate, Fig. 10. Also, in Fig.11, the effect of the spacing between the nozzle and impingement surface on the jet structure is observed. The jet spreading (jet width) and the decay of the main velocity are affected by varying the angle between the two plates as well as the spacing between the nozzle and plates.

5. CONCLUSIONS

An air jet was allowed to impinge on two flat plates with an angle between them. The jet behavior was investigated by varying the nozzle to plate spacing, stagnation pressure ratio, and the angle between the two plates. The total pressure distribution in the region between the nozzle and impingement surface was measured using a pitot tube and static wall pressure distribution along the impingement surface was measured using pressure tabs made on the impingement surface. These measurements are intended to gain understanding the pressure profile through the region between the nozzle and plates and over the plate surface, since the pressure distribution affects the flow structure of the impinging jets. Navier-Stokes equations with a k-ε model were solved to correlate the jet behavior. Results reveal that the pressure profile is practically independent of the angle θ, but is dependent on stagnation pressure and nozzle to plate spacing. The wall pressure is a maximum at the stagnation point and decreases with increasing the distance x/b. As the stagnation pressure increases, the maximum pressure increases every where. The pressure distribution shows a small region of lower pressure near the jet periphery, where the static pressure in that region is slightly smaller than the ambient pressure, which is most evident in the region of $1 \leq x/b \leq 2$. The pressure recovery is inevitable since momentum must be conserved. The computed results were shown to accurately predict the flow jet behavior over the surface. Complex features like separation and reattachment on the surface strongly influence the wall pressure distributions. Additionally, experimental and numerical results are in reasonable agreement within the impingement region.

6. REFERENCES

[1] Chen, M., Chalupa, R., West, A.C., and Modi, V., "High Schmidt Mass Transfer in a Laminar Impinging Slot jet Flow", Int. J. of Heat and Mass Transfer, Vol. 43, 2000, PP. 3907-3915.

[2] Chiu, C.P., and Kuo, Y.S., "Numerical Study of rge Turbulent Heat Transfer in a Motorized Engine Utilizing a Two Boundary Method Grid Generation Technique", Numerical Heat Transfer, Part A, Vol. 28, 1995, PP. 215-230.

[3] Chupp, R., Helms, H., McFadden, P., and Brown, T., "Evaluation of Internal Heat Transfer Coefficients for Impingement Cooled Turbine Airfoil", J. Aircraft, Vol. 6, 1969, PP. 203-208.

[4] Colucci, D.W., and Viskanta, R, "Effect of Nozzle Geometry on Local Convective Heat Transfer to a Confined Impinging Air Jet", Experimental Thermal and Fluid Science, Vol. 13, 1996, pp. 71-80.

[5] Cornaro, C., Fleischer, A.S., and Goldstein, R.J., "Flow Visualization of a Round Jet Impinging on Cylindrical Surface", Experimental Thermal and Fluid Science , Vol. 20, 1999, pp. 66-78.

[6] Gardon, R., and Akfirat, J.C., "The Role of Turbulence in determining the heat transfer characteristics of impinging jets", Int. J. Heat Mass Transfer, vol. 8, 1965, PP. 1261- 1272.

[7] Hrycak, P., "Heat Transfer From a Row of Jets Impinging on Concave Semi-Cylindrical Surfaces", Int. J. Heat Mass Transfer, Vol. 28, 1981, pp. 175-181.

[8] Hwang, C.J., and Liu, J.L., "Numerical Study of Two Dimensional Impinging Jet Flow Field", AIAA Journal, Vol. 27, No. 7, July 1989, pp. 841-842.

[9] Khodadadi, J.M. and Vlachos, N.S., "Study of Coaxial Turbulent Jets", AIAA Journal, May (1989), pp.532-541.

[10] Lee, J., and Lee, S., "Turbulent Flow and Heat Transfer Measurements on a Curved Surface with a fully developed Round Impinging Jet", Int. J. of Heat and Fluid Flow, vol. 18, 1997, pp. 160-169.

[11] Lee, S.J., Lee, J., and Lee, D., "Local Heat Transfer Measurements From an Elliptic Jet Impinging on a Flat Plate Using Liquid Crystal", Int. J. Heat Mass Transfer, Vol. 37, 1994, pp. 967-976.

[12] Lytle, D., and Webb, B.W., "Jet Impingement Heat Transfer at Low Nozzle Plate Spacing", Int. J. Heat Mass Transfer, Vol. 37, 1994, pp. 1687-1697.

[13] Parneix,S., Behnia, M., Durbin, P.A.,"Predictions of Turbulent Heat Transfer in an Axisymmetric Jet Impinging on a Heated Pedestal", Journal of Heat Transfer, vol. 121, Feb. 1999, pp. 43-49.

[14] Patankar, S.V.,"Numerical Heat Transfer and Fluid Flow", McGraw-Hill, New York, 1970.

[15] Phares, D.J., Smedley, G.T., Flagan, R.C., "The Wall Shear Stress Produced by the Normal Impingement of a Jet on a Flat Surface", J. Fluid Mech., Vol. 418, 2000, pp. 351-375.

[16] Tabakoff, W., and Clevenger, W., "Gas Turbine Blade Heat Transfer Augmentation by Impingement of Air Jets Having various Configurations", J. Eng. Power, Vol. 94, 1972, pp. 51- 60.

[17] Tam, C.K.W., and Norum, D., "Impingement Tones of Large Aspect Ratio Subsonic Rectangular Jets", AIAA Journal, Vol. 30, 1992, pp. 304-311.

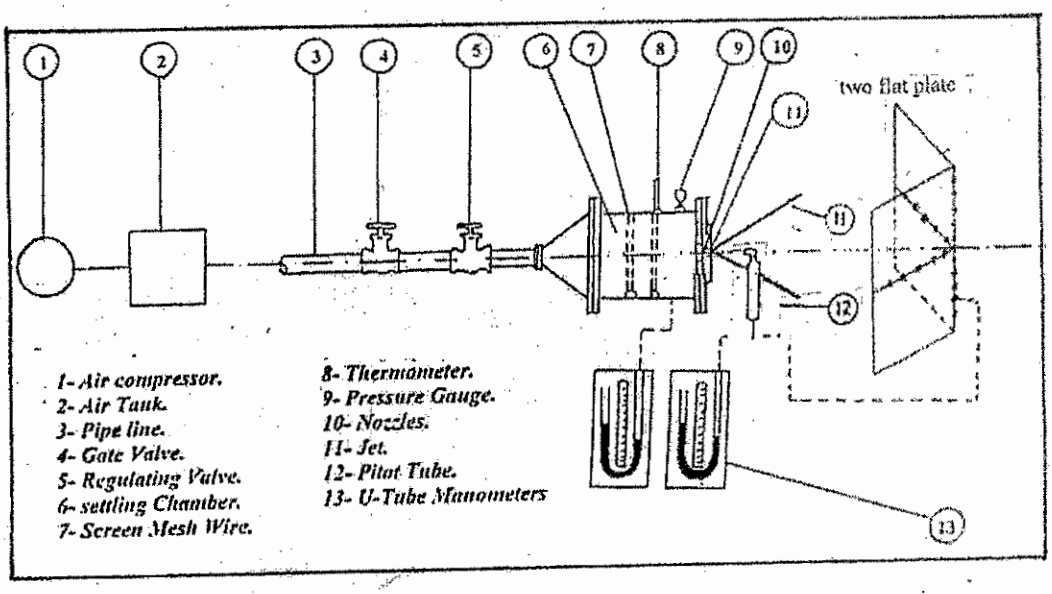

Fig. (1): Experimental set up

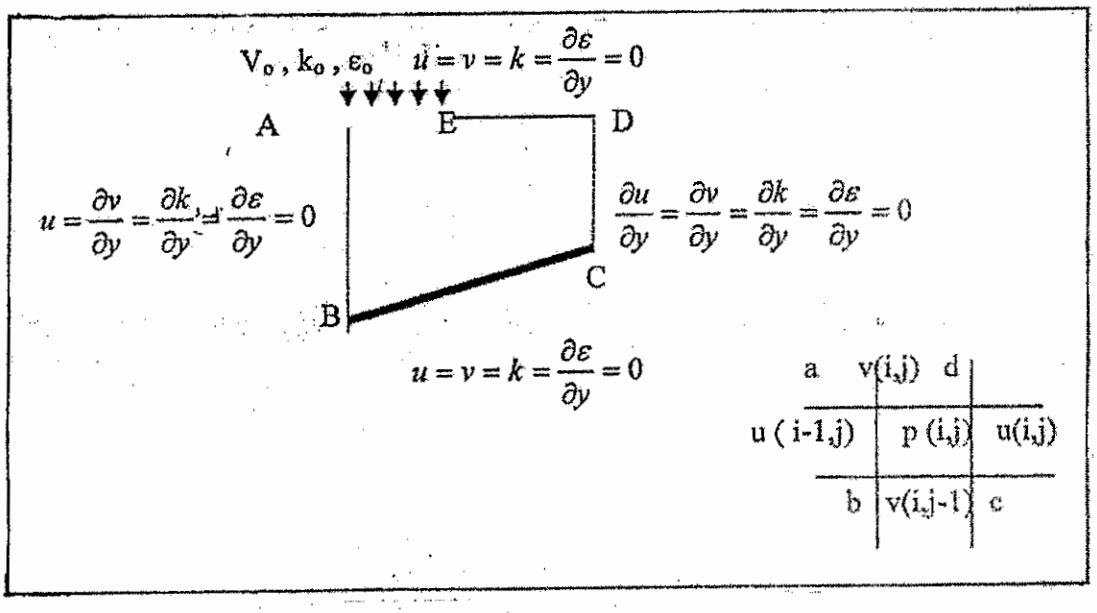

Fig.2 Boundary conditions and numerical cell

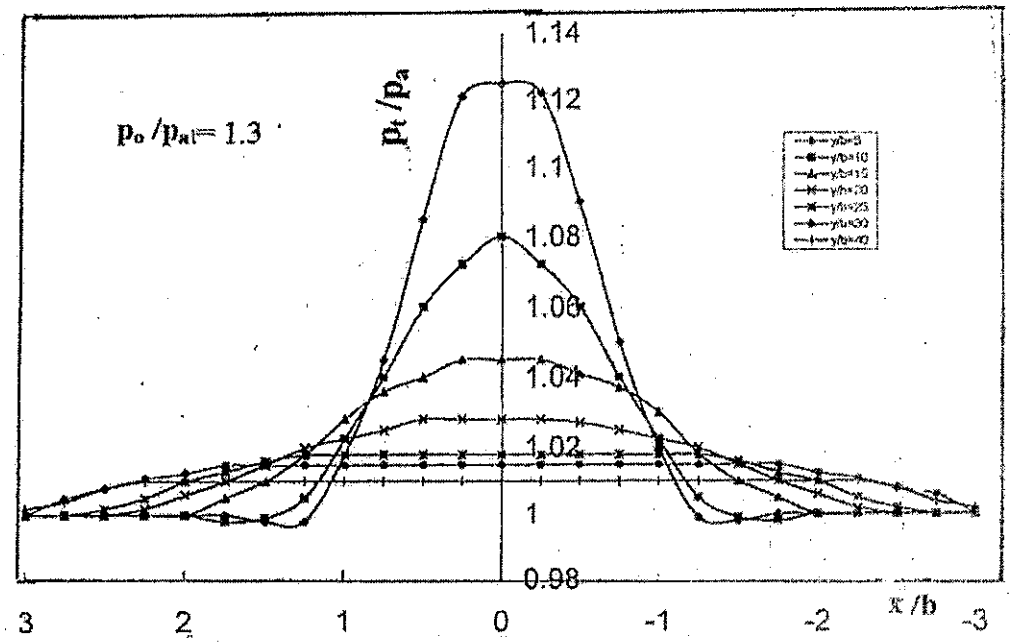

Fig.3 Distributions of total pressure

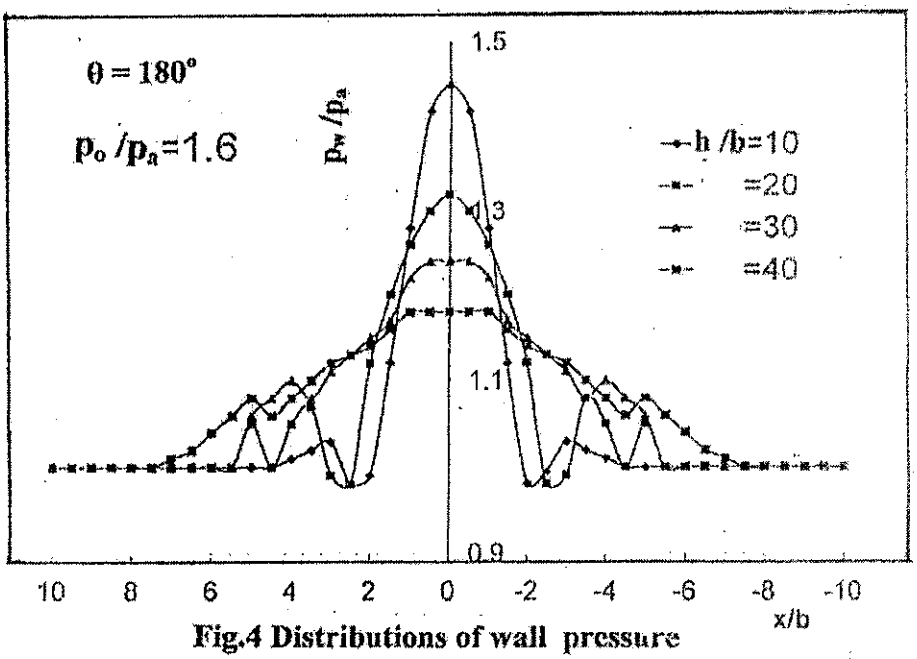

Fig.4 Distributions of wall pressure

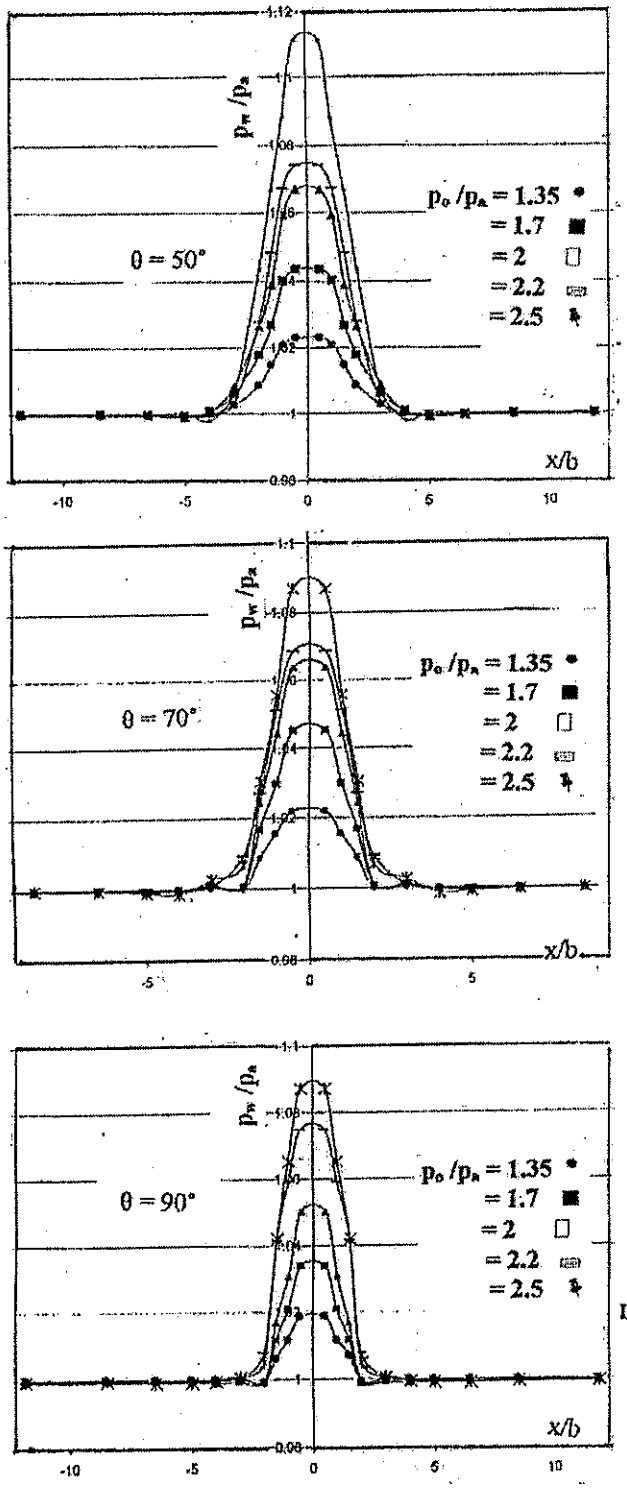

Fig.5 Effect of stagnation pressure on the wall pressure, h/b=32

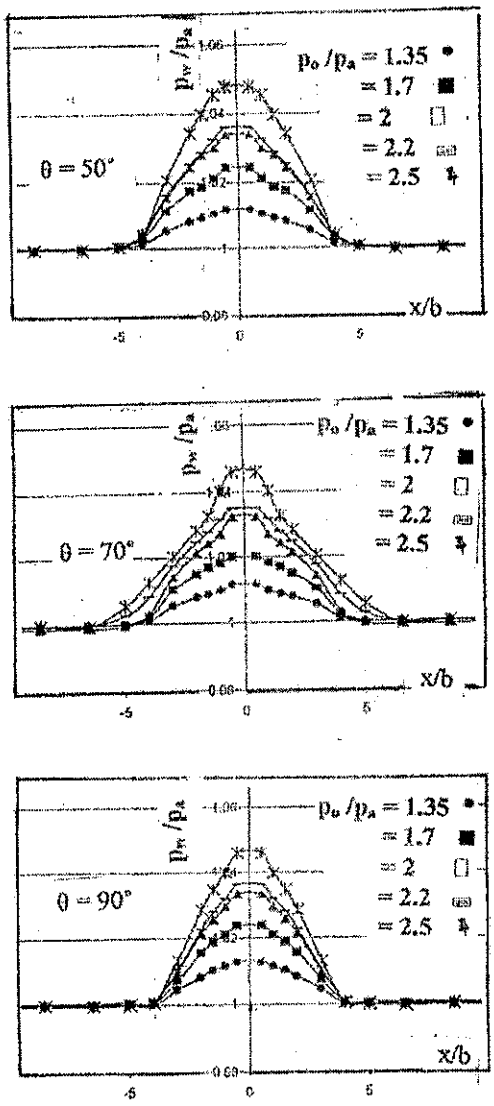

Fig.6 Effect of stagnation on the wall pressure with h/b=57

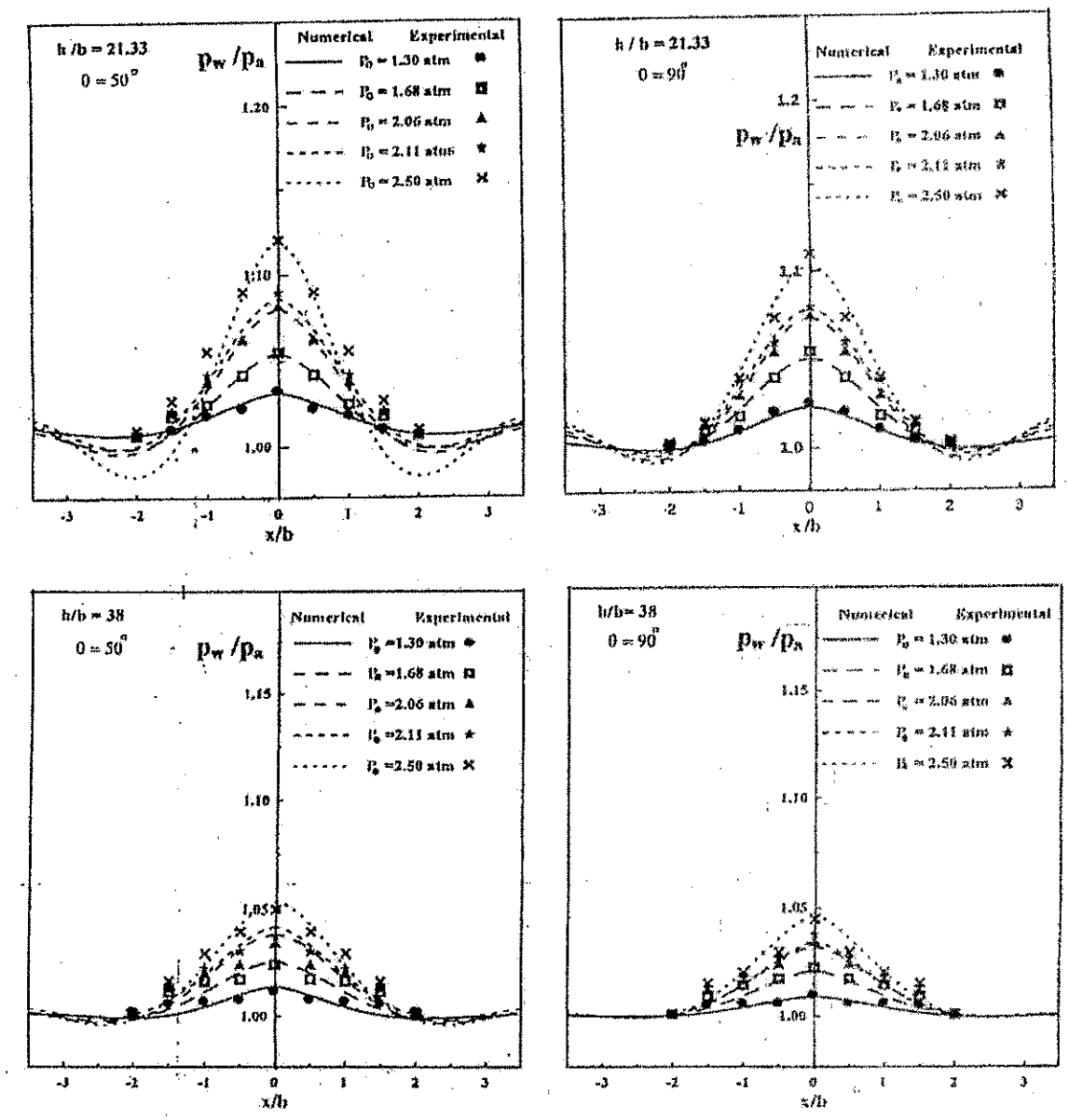

Fig.7 A comparison between experimental and numerical results

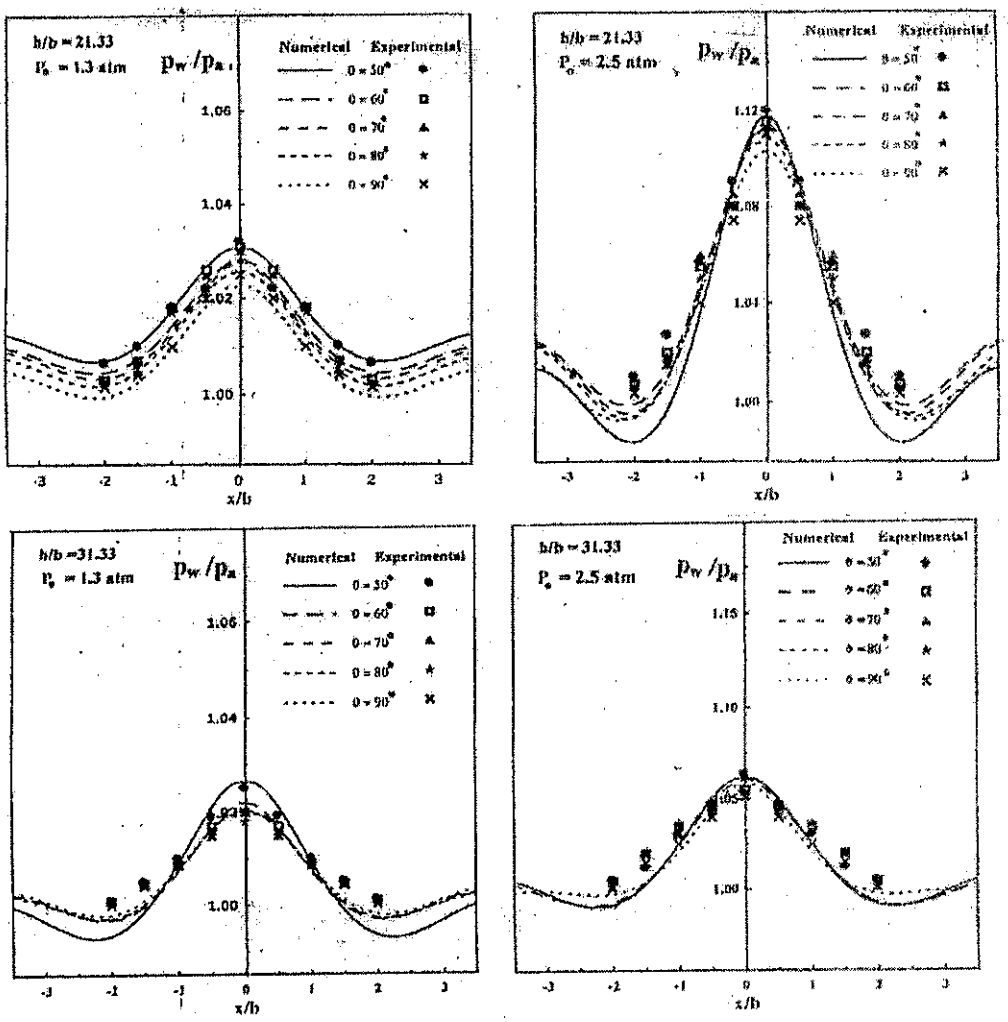

Fig.8 Effect of the angle between plates on pressure distribution, h/b=31.33

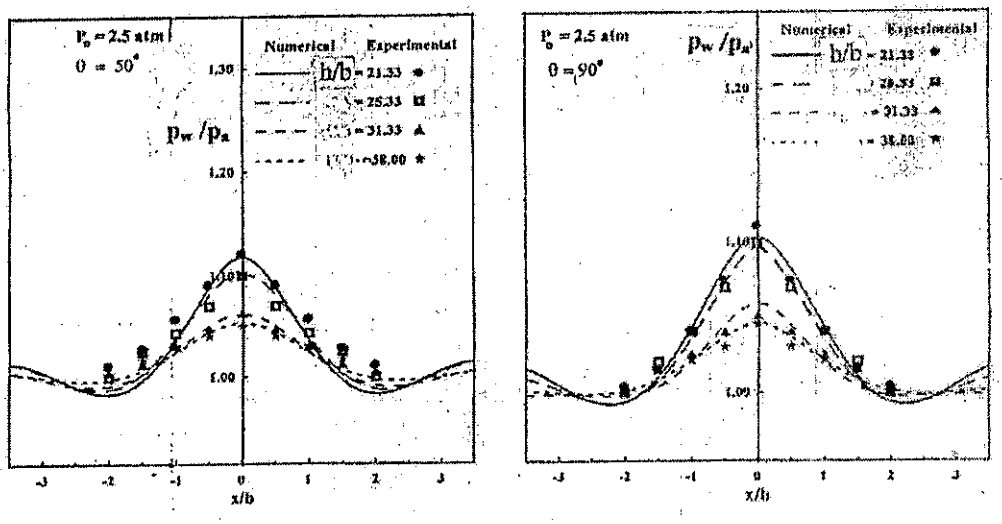

Fig.9 Effect of nozzle to plate spacing on pressure distribution

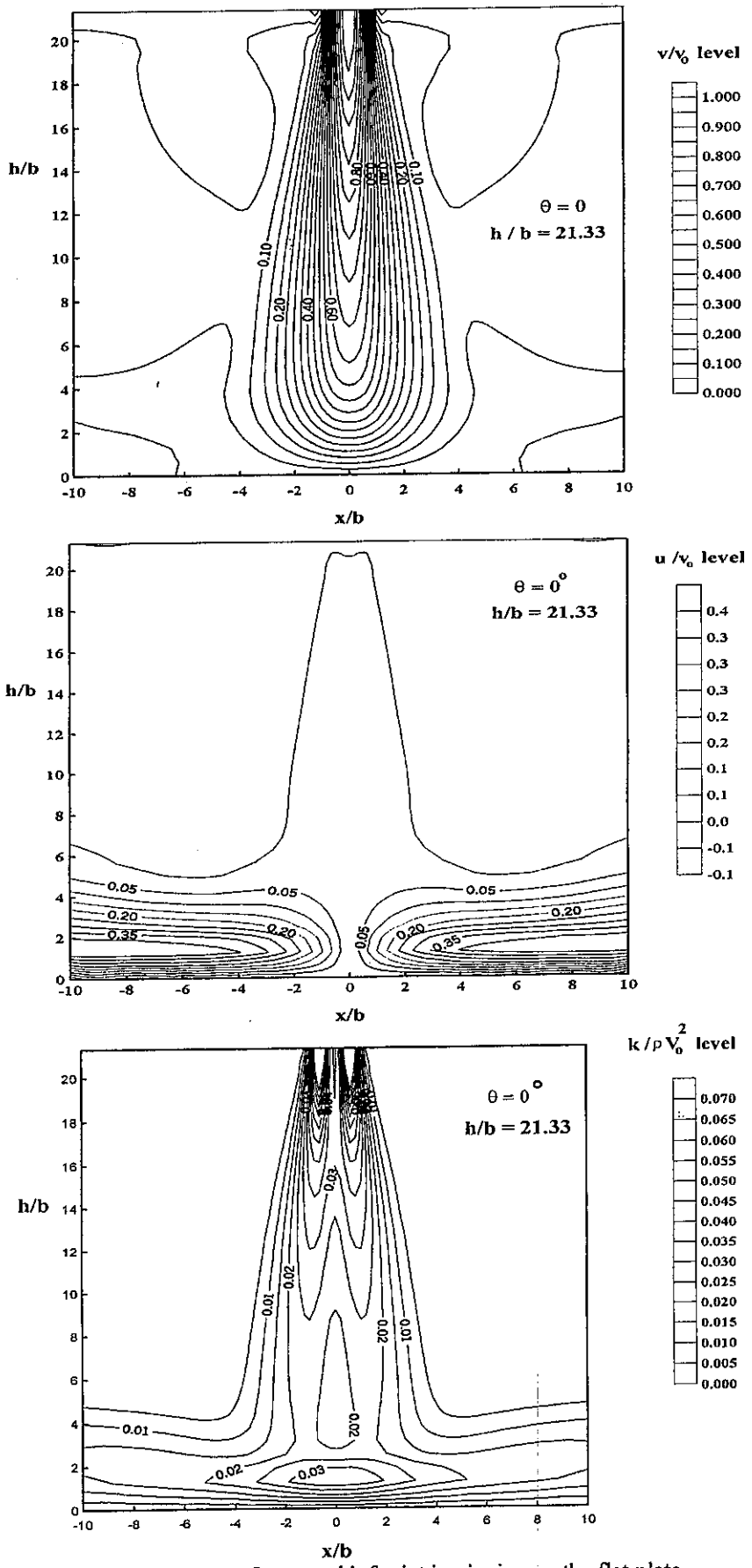

Fig 10 Contours of u, v, and k for jet impinging on the flat plate

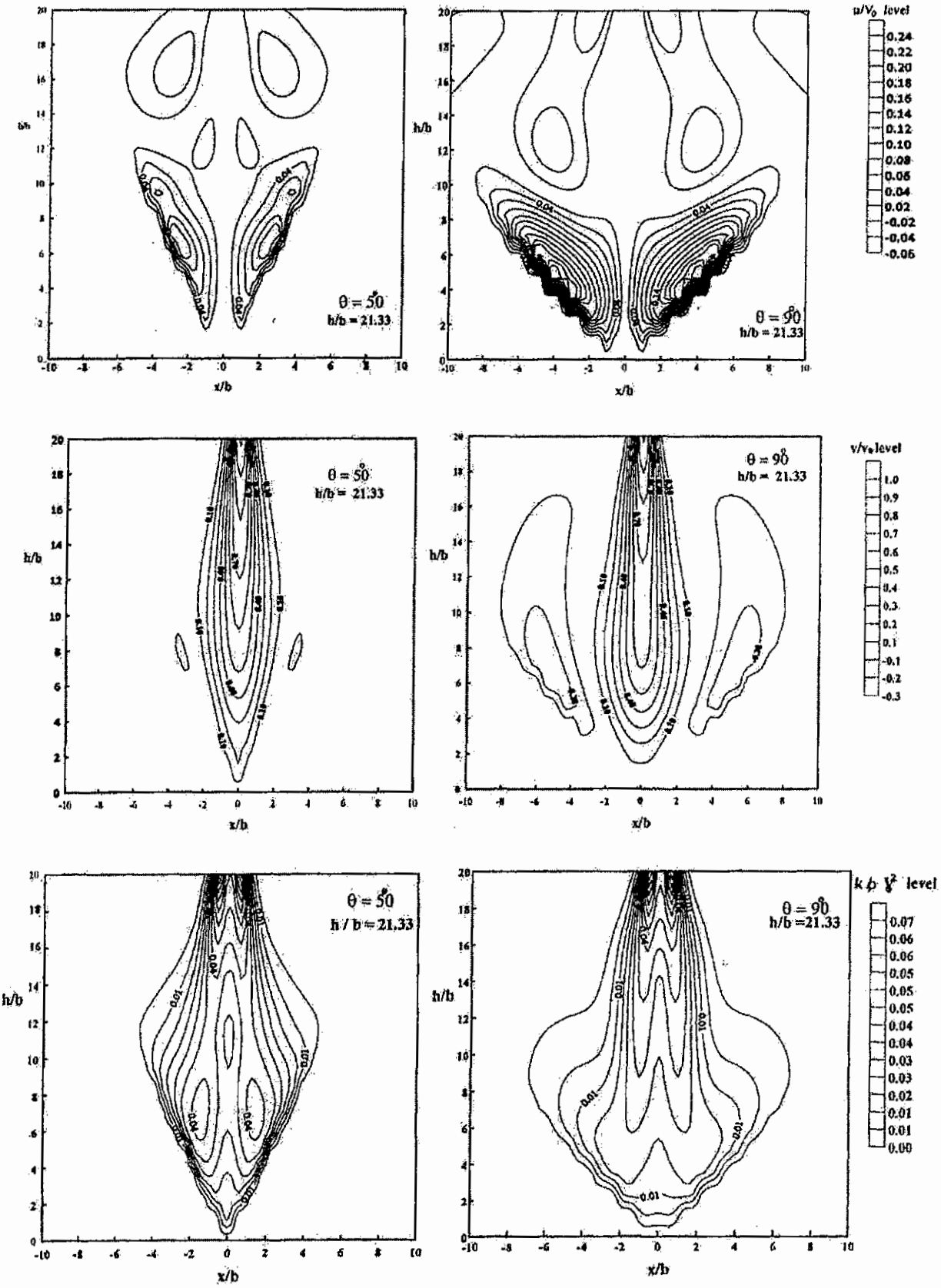

Fig. 11 Contours of u, v, and k for jet impinging on two plates with angle